2024 IEEE International Conference on Robotics and Automation (ICRA 2024)
May 13-17, 2024. Yokohama, Japan

A Detachable FBG-Based Contact Force Sensor for Capturing Gripper-Vegetable Interactions

Wenjie Lai [1,2], Jiajun Liu[1], Bing Rui Sim [1,2], Ming Rui Joel Tan [2,3], Chidanand Hegde [2,3], Shlomo Magdassi [2,4], Soo Jay Phee [1,2]

***Abstract*—Vertical farming, a sustainable key for urban agriculture, has garnered attention for its land use optimization and enhanced food production capabilities. The adoption of automation in vertical farming is a pivotal response to labor shortages, addressing the need for increased efficiency, particularly in labor-intensive tasks like harvesting. Although soft robotic grippers offer a significant promise for delicately handling fragile objects, the absence of sensors has hindered their full potential to execute precise and secure grasping. To address this challenge, we present a new solution: a detachable Fiber Bragg Grating-based flexible contact force sensor to capture gripper-vegetable interactions. The sensing module was 3D printed using soft material, and the FBG fiber was attached to the module using epoxy. From evaluation tests, this lightweight sensor demonstrated a wide measurement range of up to *9.87 N*, with a high sensitivity of *141.7 pm/N*, good repeatability, and a hysteresis of *7.96%*. Compared to commercial load cells, our sensor achieves a small measurement RMSE of *0.41 N* and a percentage error of *4.15%*. The sensor was integrated into two robotic 3D-printed soft grippers to enable real-time monitoring of dynamic contact force during vegetable harvesting in vertical farming scenarios. By reflecting contact status, this sensor provides a promising glimpse into the future of agricultural automation, enhancing operational efficiency and strengthening situation awareness and decision-making capabilities in vertical farms. Beyond agriculture, the versatility of this sensor extends to application in areas such as warehousing, logistics, and the food and beverage industry.**

***Keywords*—Force and Tactile Sensing, Soft Sensors and Actuators, Agricultural Automation.**

I. Introduction

Agriculture, serving as a cornerstone of human civilization, offers sustenance and livelihoods for billions globally. However, the ever-expanding global population and rapid urbanization exert immense pressure on available land for farming and raise concerns about food security. To optimize land use and improve agricultural productivity, sustainable urban agriculture like vertical farming [1] has gained recent popularity. To reduce labor dependency and boost efficiency, the adoption of automation is crucial, especially for tasks like seeding, sprouting, harvesting, and packaging in urban agriculture. Soft robotic grippers [2-4], inspired by nature, provide substantial potential in delicately handling fragile fruits and vegetables due to their dexterity, adaptability, and compliant characteristics [5]. Precise and secure gripping during vegetable harvesting poses a challenge, especially when crops are soiled, wet, and densely clustered — common occurrences in vertical farming environments. This highlights the necessity of gripper-crop interaction sensing. Accurately modeling the force exerted by a soft gripper is challenging due to the intricate and nonlinear dynamics of soft material. Therefore, integrating physical sensors at the tip of the soft gripper is crucial to improve safety and situation awareness during robot operations. However, it is worth noting that most soft robotic grippers in the industry currently lack such sensors. To address this challenge, we aim to develop a contact sensor that can be easily attached to soft grippers to provide valuable interaction force data.

Since 2017, there has been a rising trend in research focused on employing soft grippers for crops [6], especially for harvesting apples [7], tomatoes [8], and berries [9]. These grippers are often actuated using electric motors or through the application of positive (pneumatic) and negative (vacuum) pressure to execute various actions like grabbing, pulling, and twisting in crop harvesting. The majority of soft grippers exert a maximum contact force on crops within the range of *10 N* [6], while a subset can generate even greater force exceeding *20 N* [10]. While soft grippers help minimize crop damage during grasping, the absence of force feedback limits their ability to assess contact conditions, potentially leading to scratches and bruises [7].

Consequently, for non-destructive harvesting and crop sorting, recent research has seen a growing inclination towards integrating various sensors including resistive, piezoresistive, magnetic, capacitive, and optical sensors, into soft grippers [11]. In 2023, A. Qiu *et. al* integrated a near-infrared (NIR) based sensor to detect the ripeness of blackberries [9]. In 2022, S. Q. Liu *et. al* introduced a novel GelSight sensor (*2.5 mm* x *18 mm* x *25 mm*) by embedding LEDs, a laser-dotted thin layer, and a camera into a Fin-Ray inspired soft finger, to realize tactile sensing for state-estimation [12]. In 2019, L. Scimeca *et. al* incorporated six capacitive tactile sensing units into each gripper finger to differentiate the flesh stiffness and ripeness of mangos, operating within the linear range of the

This research is supported by the Smart Grippers for Soft Robotics (SGSR) Programme (grant number: 021990-00011) under the National Research Foundation, Prime Minister's Office, Singapore. It is part of the Campus of Research Excellence and Technological Enterprise (CREATE) Programme.

Affiliation:
1. School of Mechanical and Aerospace Engineering, Nanyang Technological University, Singapore.
2. Singapore-HUJ Alliance for Research and Enterprise (SHARE), The Smart Grippers for Soft Robotics (SGSR) Programme, Campus for Research Excellence and Technological Enterprise (CREATE), Singapore.
3. School of Materials Science and Engineering, Nanyang Technological University, Singapore.
4. Casali Center for Applied Chemistry, Institute of Chemistry, The Hebrew University of Jerusalem, Israel.
Corresponding author:
W. Lai (wjlai@ntu.edu.sg; laiw0021@e.ntu.edu.sg).

sensor from *0* to *5.5 N* [13]. It is important to highlight that many electrical sensors present certain challenges when integrating them into soft grippers, in terms of their physical size, integration complexity, signal processing, rigid substrates, transmission loss, susceptibility to environmental factors like light condition, temperature variation, humidity and vibration, which can potentially affect their sensing capability. Additionally, some of these sensors may exhibit limitations of sensing resolution and measurement range.

Recently, there has been a trend in utilizing Fiber Bragg Grating (FBG) sensors [14-18] for force sensing and shape sensing in soft gripper/material due to their excellent signal-to-noise ratio (SNR), high sensitivity, tolerance of vibration, corrosion resistance, and electrical passivity [19]. Unlike other types of optical fiber sensors, FBG sensors exhibit structural simplicity and remain little affected by challenges associated with phase discontinuity or fluctuations in intensity [20]. In 2023, J. Hao *et. al* combined FBG sensor with two tiny nitinol rods to enhance high strain transfer to realize shape sensing of a pneumatically driven soft finger. This innovation has a remarkable bending deformation and the sensor measurement range is up to *320 degrees* [15]. In 2021, Y. He *et. al* accomplished shape sensing in soft robots by using a helically embedded stretchable FBG-based sensor, with a body elongation of *56.2%* and a bending angle of up to *160 degrees* [16]. In 2020, Li *et. al* used parallel dual FBG arrays to realize real-time curvature sensing and shape reconstruction of a cable-driven soft manipulator [17]. In 2019, J. Feng *et. al* embedded FBG fiber within a silicone rubber body to create a slip sensor for robotic fingertip. This sensor can detect the roughness of different materials, including sandpaper, cardboard, and plastic board [18]. These research endeavors underscore the promising potential of FBG technology in advancing the safe and precise control of soft robotics in agriculture area. The cross-sensitivity of FBG sensors to temperature in farm environments can be offset by using dual FBG array method [21].

To capture contact information between the soft grippers and vegetables for harvesting in vertical farming, in this paper, we introduce a new detachable flexible contact force sensor based on FBG. This 3D-printed sensing module can be effortlessly affixed to and detached from different robotic grippers. Differing from conventional FBG-based sensors that typically measure the longitudinal force along the optical fiber [22], this proposed sensing module is designed to capture the lateral force acting on the optical fiber. Model was studied to reveal the relationship between the contact force and wavelength shift. The sensor offers a wide measurement range spanning from *0 N* to *9.87 N*, with a high sensitivity of *141.7 pm/N*. It shows good repeatability, with a hysteresis of *7.96%*. Compared to commercial load cells, our sensing module exhibits a root-mean-square-error (RMSE) of *0.41 N* and a relatively low percentage error of *4.15%* in measurement. To assess real-world applicability, our sensor, integrated to two types of pneumatically driven 3D-printed soft grippers mounted on a *UR5e* robotic arm, reflected the interactions between the gripper and vegetables during the loofah and Bok Choy harvesting process in vertical farming environments.

The paper is organized as follows. *Section II* introduces the design, fabrication, and a calibration model of the sensing module. Experimental setup used to verify the modeling and to evaluate the performance of the sensing module is described as well. Furthermore, sensor integration with two different soft robotic grippers mounted on a *UR5e* robotic arm for vegetable harvesting applications is discussed. *Section III* focuses on the presentation and discussion of the results derived from a series of tests, including modeling verification, repeatability assessment, comparison studies, hysteresis analysis, and application demonstrations. Finally, *section IV* concludes the paper and outlines our future work.

II. Methodology

A. Design and Fabrication of Contact Force Sensor

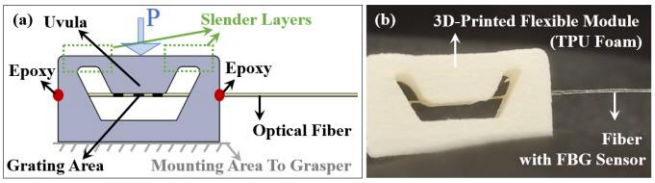

Figure 1. (a) Design of the flexible sensing module; (b) Fabricated flexible sensing module.

A flexible FBG-based sensing module *(Figure 1a)* was designed to measure the contact force, i.e., a lateral force *P* applied to the FBG optical fiber. The bottom surface of the sensing module serves as the mounting area to graspers using adhesive material. A prototype of this lightweight sensing module *(Figure 1b)* was printed using TPU foam material *(colorFabb varioShore TPU)* by a 3D printer (*Original Prusa i3 MK3*). The printing parameters were configured as follows: nozzle diameter: *0.4 mm*; nozzle temperature: *230 °C*; printing bed temperature: *60 °C*; layer height: *0.2 mm*; printing width: *0.6 mm*.

This standalone sensing module has a length of *15 mm*, a width of *10 mm*, and a height of *8 mm*. Two ends of the FBG optical fiber (CW: *1550±0.5nm*; FWHM: *0.4±0.1nm*; reflection > *70%*; *polyimide* recoating; *FC/APC* connector) were attached to the side supports of the module using epoxy *(UHU Epoxy Ultra Strong)*. A pretension was applied to the optical fiber to prevent slacking during the curing process of the epoxy. The grating area was positioned directly beneath the uvula of the module, nestled within a groove of the uvula structure. The slender layers (thickness: *1 mm*) introduced flexibility for uvula deformation, complemented by a *2.5-mm* gap between the uvula and the lower surface of the sensing module, creating ample space for deflection to occur.

Upon the application of contact force (specifically, lateral force) to the upper surface of the sensing module, the uvula descended, exerting pressure on the optical fiber and inducing longitudinal deformation along its length. The deformation along the highly sensitive FBG sensor was further transferred to wavelength shift, recorded in real-time by an interrogator *(Luna HYPERION si255)*. In the subsequent subsection, we delve into the modeling study of the sensing module, unveiling the connection between the wavelength shift and contact force.

B. Modeling Study: Contact Force v.s Wavelength Shift

In our modeling approach for the fiber deformation within the sensing module (*Figure 2a*), we simplified the scenario by

treating it as a concentrated load applied to an Euler–Bernoulli beam fixed at both ends [23]. In this model, the gravity of the optical fiber is negligible. The Young's modulus of the slender layers (*TPU foam*) is *22.44 MPa*, compared to *13.75 GPa* of the coated single mode fiber (*SMF*). The significant difference in stiffness underscores the flexibility of the slender layer, making it highly adaptable for bending, thus ensuring efficient transmission of the contact force to the fiber. As illustrated in *Figure 2b*, the fixed supports on the optical fiber, where epoxy is applied, are designated as points *A* and *B*; The original length of the fiber between these two supports is denoted as $AB = L$; Point *C* represents the midpoint of this length, i.e., $AC = BC = L/2$; A contact force *P* (point load) is applied to the top surface of the sensing module, leading to the deformation of the optical fiber as shown by the curve *ADB*, i.e. *L'*; Point *D* is the midpoint of the curve *ADB*; The Young's modulus of the coated single mode fiber is *E*; The diameter of the fiber is *d*, and the area inertia property for the fiber is $I = \pi d^4/64$. The maximum deflection occurs at the midpoint of the beam, i.e., $CD = PL^3/(192EI)$.

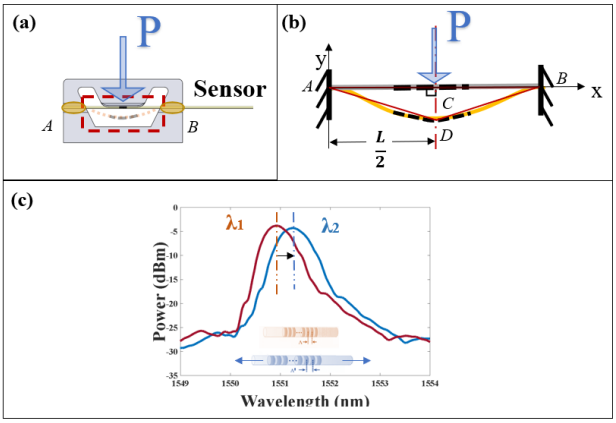

Figure 2. Schematic diagram: (a) Fiber deformation in the sensing module due to the applied contact force P; (b) Revealing relationship between the contact force and the fibre deformation; (c) FBG working principle.

We estimate that the curve length *ADB* is approximated to the sum of the lengths of *AD* and *BD* of $\triangle CDA$ and $\triangle CDB$, i.e., $\overline{ADB} = AD + BD$. Then, we determined the deformed length as in *(1)*:

$$L' = 2\sqrt{AC^2 + CD^2} = L\sqrt{1 + \frac{P^2 L^6}{9216E^2 I^2}} \quad (1)$$

The FBG, a short optical fiber segment with periodic refractive index variation, reflects light with a wavelength of $\lambda_B = 2n_{eff}\Lambda$ that shifts due to temperature and strain (*Figure 2c*). n_{eff} is the effective refractive index of the fiber core mode and Λ represents the core refractive index modulation. n_{eff} and Λ are dependent on temperature change ΔT and axial strain change $\Delta\varepsilon$. The Bragg wavelength shifts with respect to strain and temperature variations [24]. For a common silica fiber, the typical values are $K_T = 10\ pm/°C$ and $K_S = 1\ pm/\mu\varepsilon$ respectively.

$$\frac{\Delta\lambda_B}{\lambda_B} = K_T \Delta T + K_S \Delta\varepsilon \quad (2)$$

We did experiments in a laboratory room where the temperature remained constant, i.e., $\Delta T = 0$. Thus, we have:

$$\Delta\varepsilon = \frac{\Delta\lambda_B}{k_S\lambda_B} = \frac{L' - L}{L} \quad (3)$$

After setting constant values as $c_1 = k_S\lambda_B$ and $c_2 = L^6/(9216E^2I^2)$, the following equation is derived from *(1)* to *(3)*:

$$\Delta\lambda_B = c_1(\sqrt{1 + c_2P^2} - 1) \quad (4)$$

which reveals the relationship between the wavelength shift $\Delta\lambda_B$ of the FBG sensor and the applied contact force *P*. Subsequently, we can obtain the calibration equation as follows:

$$P = \sqrt{\frac{(\frac{\Delta\lambda_B}{c_1} + 1)^2 - 1}{c_2}} \quad (5)$$

C. Model Verification and Performance Test Platform

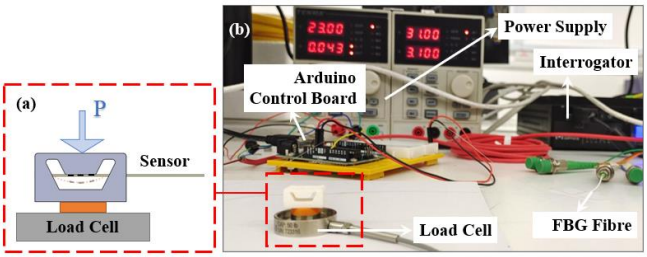

Figure 3. (a) The schematic diagram for force calibration; (b) Test platform.

A series of tests were carried out to verify the modeling equation *(4)* and assess the performance of the sensing module, in a sequence of repeatability test, comparison study, and hysteresis study. The modeling verification test was conducted to show the alignment of the relationship between the contact force *P* and the wavelength shift $\Delta\lambda_B$ with *equation (4)*, as derived in the previous subsection. Performance tests for repeatability, comparison study, and hysteresis analysis were also carried out to evaluate the effectiveness of our proposed sensing module.

In the test platform *(Figure 3)*, we positioned a load cell *(Futek, LTH 300)* at the base of the sensing module to capture the transmitted contact force. As contact force was applied to the top surface of the sensing module, the load cell recorded the force *P* and data was collected through a control board *Arduino Uno*, while simultaneously the interrogator captured the corresponding wavelength shift $\Delta\lambda_B$ of the FBG. Results of model verification test, repeatability test, comparison study, and hysteresis test can be found in *subsection III.A* to *subsection III.B*.

D. Application Setup in Vertical Farming Scenario

Exploring the viability and practicality of the flexible sensing module, we integrated it with two types of pneumatic-driven 3D-printed soft robotic grippers and mounted the grippers on a robotic arm *(UR5e)* for vegetable harvesting in a vertical farming scenario *(Figure 4a)*. The detachable sensor was affixed to a tweezer-type gripper for loofah harvesting and subsequently transferred to a finger-type gripper for Bok Choy harvesting. A double-side

sticker was employed to attach the mounting area of the sensor module to the grippers.

The tweezer-type gripper *(Figure 4b)* was assembled by inserting two tweezers into slots of a compressible pneumatic chamber. The tweezers were printed using *Stratasys Objet 260 Connex3* 3D Printer. The compressible pneumatic chamber was 3D printed using *Resione F69* resin through a DLP (Digital Light Processing) printer (*Anycubic photon D2*). The tweezer contains a cavity at its tip for hosting the FBG sensor.

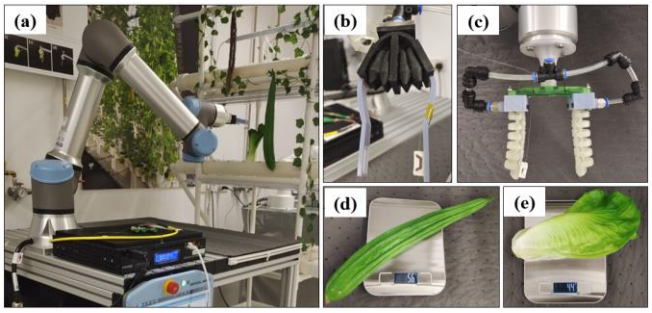

Figure 4. Sensor application for vegetable harvesting in vertical farming scenarios: (a) Application Setup; (b) Sensor mounting on the pneumatic tweezer-type gripper; (c) Sensor mounting on the pneumatic finger-type; (d) Weight of the artificial loofah; (e) Weight of the artificial Bok Choy.

For the finger-type gripper *(Figure 4c)*, its continuum pneumatic finger was printed using a 3D printer (*Anycubic Photon Ultra, 395 nm*) with formulated resin consisting of *49.5 wt%* (aliphatic urethane diacrylate diluted by *30-35%* isobornyl acrylate (*Ebecryl 8413, Allnex*)), *49.5 wt%* acrylate ester produced from Neo-decanoic acid, 2-oxyranylmethylester and 2-propenoic acid (*Ebecryl 113, Allnex*), and *1 wt%* Phenylbis (*2,4,6-trimethylbenzoyl*) phosphine oxide. Each layer was irradiated for five seconds, with a layer thickness of *50 μm*. Subsequently, the printed structures were sonicated with isopropyl alcohol (*IPA*) for three minutes to remove any uncured monomer. The cleaned pneumatic fingers were then dried in a vacuum oven at *60 °C* for two hours before exposuring to *405 nm* light with constant rotation in *Anycubic Wash & Cure plus* machine for one hour.

The artificial vegetable weights are *56 grams* for loofah and *44 grams* for Bok Choy, within the weight range of actual vegetables *(Figure 4d* to *Figure 4e)*. During the pick-n-place demonstrations, the interaction force between vegetables and grippers were captured by our flexible sensing module, which can be found in *subsection III.C*.

III. Results and Discussion

A. Model Verification

Two rounds of load-unloading tests were carried out to verify the modeling equation in subsection III.B. Data fitted well with equation $\Delta\lambda_B = 110 \cdot (\sqrt{1 + 1.54P^2} - 1)$, with R-square of *0.975 (Figure 5)*. The equation is aligned with our modeling equation *(4)*. The calibration equation *(5)* to convert wavelength shift into contact force then becomes $P = \sqrt{\frac{(\frac{\Delta\lambda_B}{110} + 1)^2 - 1}{1.54}}$.

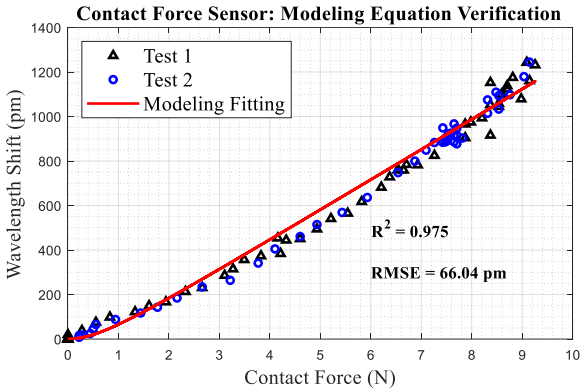

Figure 5. Verification result of modeling equation for contact force sensor.

The RMSE of *66.04 pm* between the test data and our modeling fitting data is mainly caused by curve elongation approximation. Also, instead of a single point contact force, the force applied to the top surface might be uniformly distributed from the uvula to the optical fiber, contributing to the error of the modeling as well.

B. Sensor Performance Assessment

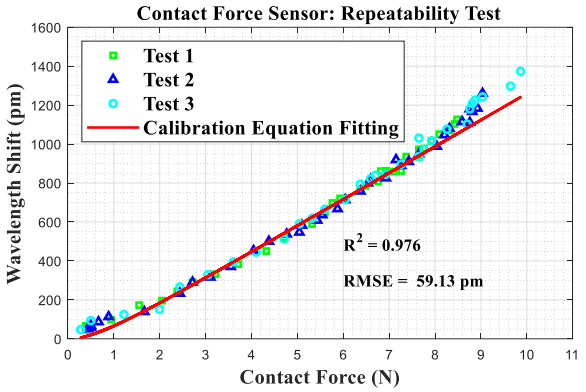

Figure 6. Repeatability test result of the contact force sensor.

In line with the experimental setup described in *subsection II.C*, we performed another three runs of loading and unloading tests, expanding the force range to *9.87 N* and wavelength shift to *1397.9 pm*, to assess the repeatability of the fabricated sensor. The sensor presented a high sensitivity around *141.7 pm/N*. The interrogator (*Luna HYPERION si255*) resolution is *1 pm* and the noise is around *3 pm*. Thus, for the contact force sensor, the resolution is *~1/141.7 = 0.007 N,* and the signal-to-noise ratio is *~3/141.7 = 0.02 N*.

The measurement range of this sensor covers the maximum contact force typically encountered by most soft grippers when handling crops [6]. The test results closely overlapped, demonstrating good repeatability of the sensor *(Figure 6)*. Furthermore, the calibration equation obtained from the preceding subsection exhibited a solid fit to the test data, yielding an R-square of *0.976* and RMSE of *59.13 pm*.

By utilizing the calibration equation obtained in *Section III.A* to convert the wavelength shift to contact force, we did a comparison study of our FBG-based sensing module against the load cell. The study showed an RMSE of *0.41 N* over a force range from *0* to *9.87 N*, indicating a measurement percentage error of approximately *4.15% (Figure 7)*. There are some peak force differences. The difference in

measurement occurs during the unloading phase, attributed to hysteresis effects of our fabricated sensor.

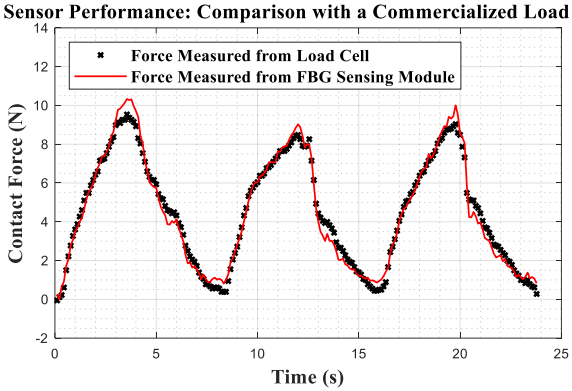

Figure 7. Comparison study between the FBG-based sensing module and the commercialized load cell sensor.

Following this, we conducted a loading-and-unloading procedure within 10s, which unveiled a peak hysteresis percentage of *7.96%* occurring at *8.3 N (Figure 8)*. The observed hysteresis phenomenon in the sensor can be caused by the inelastic characteristics of the 3D-printed material [25] and the epoxy used in fabrication. To address this issue, we recommend considering options such as altering the TPU 3D-printing material or the epoxy or modifying the attachment method as discussed in the section of future works.

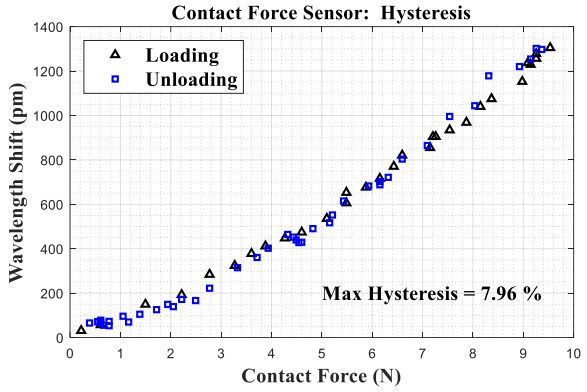

Figure 8. Hysteresis test result of contact force sensor

C. *Vegetable Harvesting in Vertical Farming Scenario*

The process to mimic loofah harvesting involved the following steps: (a) the robotic arm moved to the pick-up location *(Figure 9a)*; (b) The tweezer-type gripper firmly grasped the upper third of the loofah *(Figure 9b)*; (c) The gripper plucked the loofah from the vertical farming frame *(Figure 9c)*; (d) During the transition from the frame to the table, the orientation of the loofah changed and touched the table gently *(Figure 9d)*; (e) The robotic arm then positioned itself further downwards *(Figure 9e)*; (f) Finally, the gripper released the loofah onto the table *(Figure 9f)*.

The wavelength shifts were continuously captured by the flexible sensing module in real time, reflecting the contact force information *(Figure 10)*. Here is the detailed description of the recorded data: from time *a* to time *b*, the contact force increased from *0 N* to *2.18 N* and gradually decreased to reach a saturation level of *1.43 N* when the gripper grasped the loofah. At time *c*, the contact force suddenly spiked up to *1.65 N* when the loofah was plucked. The spike force can be due to shear force, which caused the uvula to shift a bit. Moving to time *d*, the contact force gradually climbed up to *1.75 N* and then slid down to *1.43 N* as the orientation of the loofah changed and one end of the loofah gently touched the table when the robot moved from frame to the table. At time *e*, the contact force experienced a sharp peak, reaching *1.96 N* when the robotic arm moved further downwards. Since one end of the loofah was already touched with the table, when the robotic arm further moved downwards, resistance occurred and that was detected by the sensor as a sharp peak. Finally, at time *f*, the contact force rapidly decreased as the gripper released the loofah.

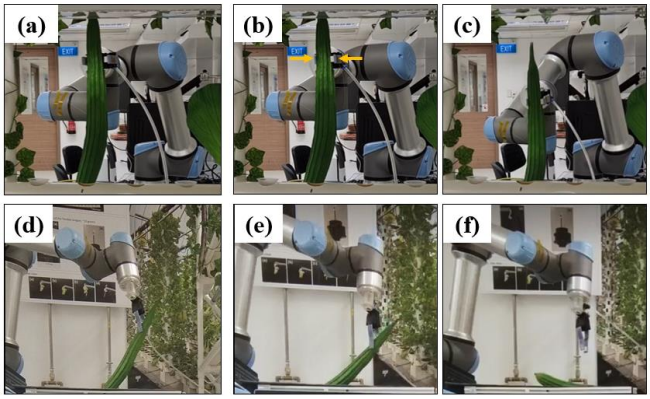

Figure 9. Loofah harvesting using a pneumatic-driven tweezer-type gripper: (a) The robot went to pick-up location; (b) The gripper grasped the loofah; (c) The robot plucked the loofah; (d) Orientation of the loofah changed; (e) The robotic arm descended further; (f) The gripper released the loofah.

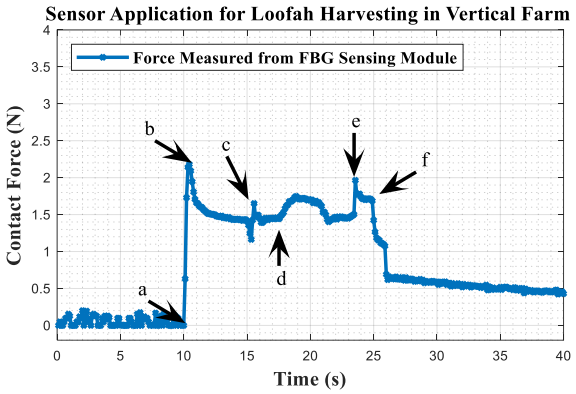

Figure 10. Force reading from FBG-based sensing module during the loofah harvesting process: a for step (a); b for step (b); c for step (c); d for step (d); e for step (e); f for step (f) in Figure 9.

The process to mimic Bok Choy harvesting involved the following steps: (a) the robotic arm moved to the pick-up location *(Figure 11a)*; (b) The finger-type gripper grasped the lower third of the Bok Choy until the gripping is secure *(Figure 11b)*; (c) The gripper picked up the Bok Choy from the vertical farming frame *(Figure 11c)*; (d) The robotic arm moved to the collection table and then positioned itself further downwards *(Figure 11d)*; (e) Finally, the gripper released the Bok Choy onto the table *(Figure 11e)*.

The wavelength shifts were continuously captured by the flexible sensing module in real time, reflecting the contact force information *(Figure 12)*. Here is the detailed description

of the recorded data: from time *a* to time *b*, the contact force increased from *0 N* to *0.53 N* when the soft finger just touched the Bok Choy and gradually increased to reach a saturation level of *0.81 N* when the gripper grasped further to ensure a secure gripping at time *c*. At time *d*, the contact force suddenly spiked up to *1.40 N* when the Bok Choy was picked up from the frame. The spike force can be due to shear force, which caused the uvula to shift slightly. During the transition from the frame to the table, the grasping force gradually dropped to a saturated level of *1.11 N*. Finally, at time *e*, the contact force rapidly dropped to *0 N* as the gripper released the Bok Choy.

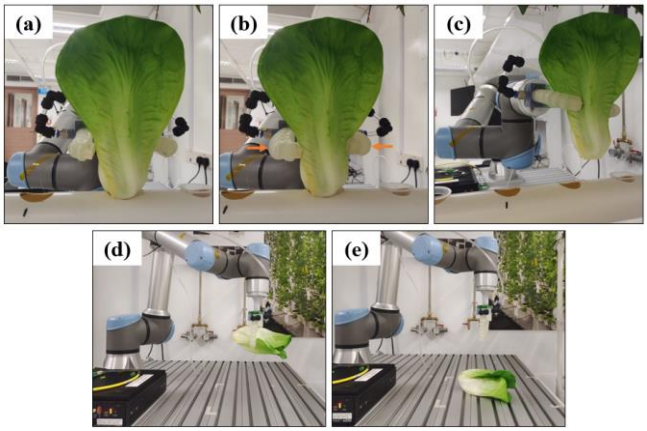

Figure 11. Bok Choy harvesting using a pneumatic finger-type gripper: (a) The robot went to pick-up location; (b) The gripper grasped the Bok Choy; (c) The robot picked up the Bok Choy; (d) The robotic arm descended further; (e) The gripper released the Bok Choy.

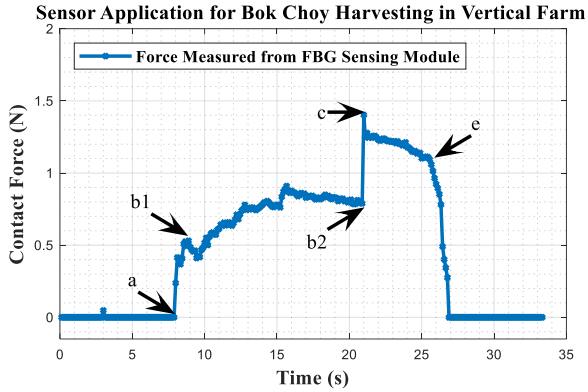

Figure 12. FBG-based sensing module's reading for Bok Choy harvesting. a for step (a); b1-b2 for step (b); c for step (c); e for step (e) in Figure 11.

In the application study, during the continuous real-time contact force measurement, we observed that the flexible sensing module could deliver sharp peak signals to indicate situational awareness during actions such as plucking, picking up, and interacting with the environment by the gripper and the grasped object. Apart from agricultural application, the proposed detachable flexible sensing module can also be utilized in robotic grippers for warehouse, logistics and food industries. It holds the potential to provide several advantages to the robotic system, including enhancing operational safety and reducing the risk of damage to delicate objects.

IV. Conclusion and Future Work

This paper has introduced a new FBG-based flexible contact force sensor that offers interchangeability by easily attaching to various robotic grippers, enabling the measurement of contact force on the optical fiber. The sensing module was 3D printed using soft material, and the FBG fiber was attached to the module using epoxy. Model was studied to reveal the relationship between the contact force and the wavelength shift. Tests were conducted to evaluate the performance of the sensing module. It demonstrated a high sensitivity of *141.7 pm/N*, good repeatability, and a broad measurement range from *0 N* to *9.87 N*, with a hysteresis of *7.96%*. In comparison with a commercial load cell, our sensor showed a low RMSE of *0.41 N* and a percentage error of *4.15%*. The lightweight sensor has been integrated into two pneumatically driven 3D-printed soft grippers on a *UR5e* arm to reflect the gripper-vegetable interactions during the harvesting of loofah and Bok Choy in vertical farming scenarios. Sharp peak signals were observed during actions such as plucking, picking up, and interacting with the environment by the gripper and the vegetables. By reflecting contact status, this sensor provides a promising glimpse into the future of agricultural automation, enhancing situation awareness and decision-making capabilities in vertical farms. Beyond agriculture, the versatility of this sensor extends to application in areas such as warehousing, logistics, and the food and beverage industry.

Nevertheless, current sensor evaluation has certain constraints: (i) The contact shear force and temperature fluctuations during the handling of real vegetables are expected to influence sensor performance, which is not captured using artificial vegetables; (ii) The resistance in plucking and pulling out the vegetables may vary from the real harvesting in current mock set up. To enhance the evaluation method, we aim to conduct automated vegetable harvesting in a local vertical farm, where these sensors will provide real-time interactions between the gripper and the vegetables.

Future work includes three key aspects: (i) Optimizing the sensing structure design to ensure point contact and seamless integrating the sensor into our *tendon-driven flexible robotic gripper*[1] [26] with length adjustability or other 3D-printed soft grippers. This involves embedding FBG sensors directly into finger phalanges during the 3D printing phase, utilizing *Fused Deposition Modeling (FDM)* or *Fused Filament Fabrication (FFF)* technology; (ii) Refining the current calibration model, or alternatively, conducting direct calibration using 2nd order polynomial equation; (iii) Fusing additional FBG sensors to detect the object mass and applying dual FBG array to compensate the temperature effect [21] in local vertical farms. We may implement data-driven control [27] to enhance the decision-making process, including successful grasping verification (sharp peak force as shown in point *b* in *Figure 10* and point *b1* in *Figure 12*), unexpected collision detection (force gradual increment as shown in point *d* and spike force as shown in point *e* in *Figure 10*), and preventing vegetables from slipping out of the gripper. This will ultimately lead to improved adaptability, responsiveness, and overall performance of our automatic harvesting system.

References

[1] S. H. van Delden *et al.*, "Current status and future challenges in implementing and upscaling vertical farming systems," *Nat. Food*, vol. 2, no. 12, pp. 944–956, Dec. 2021, doi: 10.1038/s43016-021-00402-w.

[1] This smart grow-and-twine gripper has been filed for a Singapore provisional patent (application number 10202302998W).

[2] Z. Xie *et al.*, "Octopus Arm-Inspired Tapered Soft Actuators with Suckers for Improved Grasping," *Soft Robot.*, vol. 7, no. 5, pp. 639–648, Oct. 2020, doi: 10.1089/soro.2019.0082.

[3] T. T. Hoang, P. T. Phan, M. T. Thai, N. H. Lovell, and T. N. Do, "Bio-Inspired Conformable and Helical Soft Fabric Gripper with Variable Stiffness and Touch Sensing," *Adv. Mater. Technol.*, vol. 5, no. 12, p. 2000724, Dec. 2020, doi: 10.1002/admt.202000724.

[4] S. Washio, K. Gilday, and F. Iida, "Design and Control of a Multi-Modal Soft Gripper Inspired by Elephant Fingers," in *2022 IEEE/RSJ International Conference on Intelligent Robots and Systems (IROS)*, Oct. 2022, pp. 4228–4235. doi: 10.1109/IROS47612.2022.9982126.

[5] E. Navas, R. Fernández, D. Sepúlveda, M. Armada, and P. Gonzalez-de-Santos, "Soft Grippers for Automatic Crop Harvesting: A Review," *Sensors*, vol. 21, no. 8, 2021, doi: 10.3390/s21082689.

[6] J. F. Elfferich, D. Dodou, and C. D. Santina, "Soft Robotic Grippers for Crop Handling or Harvesting: A Review," *IEEE Access*, vol. 10, pp. 75428–75443, 2022, doi: 10.1109/ACCESS.2022.3190863.

[7] K. Chen *et al.*, "A Soft Gripper Design for Apple Harvesting with Force Feedback and Fruit Slip Detection," *Agriculture*, vol. 12, no. 11, Art. no. 11, Nov. 2022, doi: 10.3390/agriculture12111802.

[8] A. Mohamed *et al.*, "Soft manipulator robot for selective tomato harvesting," in *Precision agriculture 19*, *Wageningen Academic Publishers,* 2019, pp. 799–805. doi: 10.3920/978-90-8686-888-9_99.

[9] A. Qiu, C. Young, A. L. Gunderman, M. Azizkhani, Y. Chen, and A.-P. Hu, "Tendon-Driven Soft Robotic Gripper with Integrated Ripeness Sensing for Blackberry Harvesting," in *2023 IEEE International Conference on Robotics and Automation (ICRA)*, May 2023, pp. 11831–11837. doi: 10.1109/ICRA48891.2023.10160893.

[10] O. Azami, K. Ishibashi, M. Komagata, and K. Yamamoto, "Development of Hydraulically-driven Soft Hand for Handling Heavy Vegetables and its Experimental Evaluation," in *2023 IEEE International Conference on Robotics and Automation (ICRA)*, May 2023, pp. 2577–2583. doi: 10.1109/ICRA48891.2023.10160629.

[11] C. Hegde, J. Su, J. M. R. Tan, K. He, X. Chen, and S. Magdassi, "Sensing in Soft Robotics," *ACS Nano*, Aug. 2023, doi: 10.1021/acsnano.3c04089.

[12] S. Q. Liu and E. H. Adelson, "GelSight Fin Ray: Incorporating Tactile Sensing into a Soft Compliant Robotic Gripper," in *2022 IEEE 5th International Conference on Soft Robotics (RoboSoft)*, Apr. 2022, pp. 925–931. doi: 10.1109/RoboSoft54090.2022.9762175.

[13] L. Scimeca, P. Maiolino, D. Cardin-Catalan, A. P. del Pobil, A. Morales, and F. Iida, "Non-Destructive Robotic Assessment of Mango Ripeness via Multi-Point Soft Haptics," in *2019 International Conference on Robotics and Automation (ICRA)*, May 2019, pp. 1821–1826. doi: 10.1109/ICRA.2019.8793956.

[14] W. Lai, L. Cao, P. T. Phan, I.-W. Wu, S. C. Tjin, and S. Jay Phee, "Joint Rotation Angle Sensing of Flexible Endoscopic Surgical Robots," in *2020 IEEE International Conference on Robotics and Automation (ICRA)*, May 2020, pp. 4789–4795. doi: 10.1109/ICRA40945.2020.9196549.

[15] J. Hao, Z. Zhang, S. Wang, and C. Shi, "2D Shape Estimation of a Pneumatic-Driven Soft Finger with a Large Bending Angle Based on Learning from Two Sensing Modalities," *Adv. Intell. Syst.*, vol. n/a, no. n/a, p. 2200324, doi: 10.1002/aisy.202200324.

[16] Yanlin He *et al.*, "Stretchable optical fibre sensor for soft surgical robot shape reconstruction," *Opt. Appl.*, vol. 51, no. 4, 2021, doi: 10.37190/oa210410.

[17] T. Li, L. Qiu, and H. Ren, "Distributed Curvature Sensing and Shape Reconstruction for Soft Manipulators With Irregular Cross Sections Based on Parallel Dual-FBG Arrays," *IEEEASME Trans. Mechatron.*, vol. 25, no. 1, pp. 406–417, Feb. 2020, doi: 10.1109/TMECH.2019.2949151.

[18] J. Feng and Q. Jiang, "Slip and roughness detection of robotic fingertip based on FBG," *Sens. Actuators Phys.*, vol. 287, pp. 143–149, Mar. 2019, doi: 10.1016/j.sna.2019.01.018.

[19] J. Qu *et al.*, "Recent Progress in Advanced Tactile Sensing Technologies for Soft Grippers," *Adv. Funct. Mater.*, vol. n/a, no. n/a, p. 2306249, doi: 10.1002/adfm.202306249.

[20] A. A. G. Abushagur, N. Arsad, M. I. Reaz, and A. A. A. Bakar, "Advances in Bio-Tactile Sensors for Minimally Invasive Surgery Using the Fibre Bragg Grating Force Sensor Technique: A Survey," *Sensors*, vol. 14, no. 4, Art. no. 4, Apr. 2014, doi: 10.3390/s140406633.

[21] W. Lai *et al.*, "An Integrated Sensor-Model Approach for Haptic Feedback of Flexible Endoscopic Robots," *Ann. Biomed. Eng.*, vol. 48, no. 1, pp. 342–356, Jan. 2020, doi: 10.1007/s10439-019-02352-8.

[22] W. Lai *et al.*, "Force Sensing With 1 mm Fiber Bragg Gratings for Flexible Endoscopic Surgical Robots," *IEEE/ASME Trans. Mechatron.*, vol. 25, no. 1, pp. 371–382, Feb. 2020, doi: 10.1109/TMECH.2019.2951540.

[23] A. Öchsner, "Euler–Bernoulli Beam Theory," in *Classical Beam Theories of Structural Mechanics*, Springer, Cham, 2021, pp. 7–66. doi: 10.1007/978-3-030-76035-9_2.

[24] W. Lai, L. Cao, J. Liu, S. Chuan Tjin, and S. J. Phee, "A Three-Axial Force Sensor Based on Fiber Bragg Gratings for Surgical Robots," *IEEE/ASME Trans. Mechatron.*, vol. 27, no. 2, pp. 777–789, Apr. 2022, doi: 10.1109/TMECH.2021.3071437.

[25] M. Wang, D. Shan, Y. Liao, and L. Xia, "Investigation of inelastic behavior of elastomeric composites during loading–unloading cycles," *Polym. Bull.*, vol. 75, no. 2, pp. 561–568, Feb. 2018, doi: 10.1007/s00289-017-2051-x.

[26] J. Liu, W. Lai, B. R. Sim, M. R. J. Tan, S. Magdassi, and S. J. Phee, "Smart Grow-and-Twine Gripper for Vegetable Harvesting in Vertical Farms," presented at the *IEEE 7th International Conference on Soft Robotics (RoboSoft)*, Apr. 2024 (Accepted).

[27] H. Choi, M. R. Cutkosky, and A. A. Stanley, "Integrated Pneumatic Sensing and Actuation for Soft Haptic Devices," *IEEE Robot. Autom. Lett.*, vol. 8, no. 11, pp. 7591–7598, Nov. 2023, doi: 10.1109/LRA.2023.3320494.